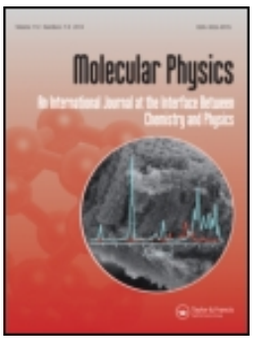

Taylor & Francis
Taylor & Francis Group

Molecular Physics

An International Journal at the Interface Between Chemistry and Physics

ISSN: 0026-8976 (Print) 1362-3028 (Online) Journal homepage: http://www.tandfonline.com/loi/tmph20

Electronically coarse-grained molecular dynamics using quantum Drude oscillators

A.P. Jones, J. Crain, F.S. Cipcigan, V.P. Sokhan, M. Modani & G.J. Martyna

To cite this article: A.P. Jones, J. Crain, F.S. Cipcigan, V.P. Sokhan, M. Modani & G.J. Martyna (2013) Electronically coarse-grained molecular dynamics using quantum Drude oscillators, Molecular Physics, 111:22-23, 3465-3477, DOI: 10.1080/00268976.2013.843032

To link to this article: http://dx.doi.org/10.1080/00268976.2013.843032

Accepted author version posted online: 27 Sep 2013.
Published online: 08 Oct 2013.

Molecular Physics, 2013
Vol. 111, Nos. 22–23, 3465–3477, http://dx.doi.org/10.1080/00268976.2013.843032

INVITED ARTICLE

Electronically coarse-grained molecular dynamics using quantum Drude oscillators

A.P. Jones[a], J. Crain[a,b], F.S. Cipcigan[a], V.P. Sokhan[b], M. Modani[c] and G.J. Martyna[a,d,*]

[a]*School of Physics and Astronomy, The University of Edinburgh, Edinburgh EH9 3JZ, UK;* [b]*National Physical Laboratory, Teddington, Middlesex TW11 0LW, UK;* [c]*Systems & Technology Group, IBM India, Bangalore, India;* [d]*Physical Sciences, IBM T. J. Watson Research Center, Yorktown Heights, New York, USA*

(*Received 29 May 2013; accepted 4 September 2013*)

Standard molecular dynamics (MD) simulations generally make use of a basic description of intermolecular forces which consists of fixed, pairwise, atom-centred Coulomb, van der Waals and short-range repulsive terms. Important interactions such as many-body polarisation and many-body dispersion which are sensitive to changes in the environment are usually neglected, and their effects treated effectively within mean-field approximations to reproduce a single thermodynamic state point or physical environment. This leads to difficulties in modelling the complex interfaces of interest today where the behaviour may be quite different from the regime of parameterisation. Here, we describe the construction and properties of a Gaussian coarse-grained electronic structure, which naturally generates many-body polarisation and dispersion interactions. The electronic structure arises from a fully quantum mechanical treatment of a set of distributed quantum Drude oscillators (QDOs), harmonic atoms which interact with each other and other moieties via electrostatic (Coulomb) interactions; this coarse-grained approach is capable of describing many-body polarisation and dispersion but not short-range interactions which must be parametrised. We describe how on-the-fly forces due to this exchange-free Gaussian model may be generated with linear scale in the number of atoms in the system using an adiabatic path integral molecular dynamics for quantum Drude oscillators technique (APIMD-QDO). We demonstrate the applicability of the QDO approach to realistic systems via a study of the liquid–vapour interface of water.

Keywords: water; quantum Drude oscillator; path integral methods; coarse-grained model; many-body dispersion

1. Introduction

Extending the variety of conditions and environments over which potential models are transferable is a grand challenge in the study of the structure of matter via computer simulation methods such as MD [1–5]. Molecules are highly electronically responsive, changing their charge distribution according to the local environment. This basic property becomes evident in complex heterogeneous systems such as biological interfaces. At such complex interfaces, electrostatic fields are different from the bulk, compromising mean-field descriptions of the charge distribution. In addition, the Coulomb fields have large gradients, leading to higher order induced moments (i.e. beyond dipole) which contribute to the forces. Lastly, the correlated quantum fluctuations of the electronic charge distributions which give rise to dispersion forces are different at interfaces, requiring post mean-field methods to capture the physics.

Current empirical model force fields typically describe long-range forces using fixed, pairwise, atom-centred Coulomb, van der Waals and short-range repulsive terms and do not generally incorporate many-body polarisation. More advanced models [6,7] based on seminal early work [8–10] include polarisation typically within the dipole approximation [11,12] and incorporate dispersion via effective pair potentials. Current *ab initio* methods appropriate for fairly large physical systems such as local density functional theory (DFT) [13,14] based MD techniques [15] reproduce polarisation responses but miss the correlation effects that give rise to dispersion. Such effects are added through a variety of techniques, which are themselves the subject of active research [16–19].

We have proposed an intermediate strategy [20–23], wherein the electronic response of an insulator is approximately reproduced by a Gaussian coarse-grained electronic structure [24,25]. A set of distributed harmonic atoms, a pseudo-electron or 'drudon' harmonically bound to a heavy pseudo-nucleus, are introduced which interact with the fixed charges in the system and other harmonic atoms via Coulombic forces. This Gaussian quasi-particle model or quantum Drude oscillator (QDO) description does not consider exchange; the light particles are treated fully quantum mechanically but are distinguishable particles which, by construction, obey Boltzmann statistics. Hence, the QDO approach breaks down at short distances and short-range, empirical, pairwise repulsive interactions are added to complete the model. However, the Born–Oppenheimer (BO)

*Corresponding author. Email: martyna@us.ibm.com

surface provided by the QDO model does yield multipole polarisabilities to all orders (many-body polarisation beyond the dipole approximation) and due to its quantum nature also yields many-body dispersion forces to all orders, albeit given by Gaussian fluctuations. The defining parameters of the QDO (charge, mass and spring constant) can be chosen to reproduce various combinations of long-range polarisation and dispersion responses of atoms, molecules or chemical moieties. The response at long-range is sufficiently accurate [23] that transferable molecular models result. Again, the QDO model is appropriate for systems of interest where there are no low-lying electronic excited states and a BO treatment is valid.

In this paper, presented in honour of Giovanni Ciccotti, professor of the structure of matter, University of Roma 'La Sapienza', and a seminal contributor to MD simulation methodology, we review the properties of QDOs and the nature of the coarse-grained electronic structure they engender. We then show that a path integral method can be used to generate QDO-based forces for on-the-fly in MD simulations with linear scaling in the number of atoms present in the system. Finally, we discuss the construction of a QDO model for water and explore the properties of the liquid–vapour interface as an exemplar heterogeneous system.

1.1. The Born–Oppenheimer surface and molecular dynamics

Underpinning the standard MD method [4] is the BO approximation. Electrons are light and fast and the nuclei are relatively heavy and slow such that the electrons can be considered to be in their quantum mechanical ground state at fixed nuclear position. The nuclei then evolve classically (as assumed here) or quantum mechanically (see, for instance, [26,27]) on the potential provided by the internuclear interactions and the ground-state energy of the electronic degrees of freedom as a function of nuclear position, i.e. the ground-state BO surface. The evolution of the electron's quantum state is therefore adiabatic, remaining in (close to) the instantaneous ground state. In this limit, by treating the nuclei classically, Hamilton's equations of motion [28] can be numerically integrated if the BO surface is known [1,2] and the structure of matter observed '*in silico*'.

In order to reach long length and time scales, the BO surface is typically approximated by a computationally efficient empirical potential [4]. Thus, covalent bonds are usually treated as rigid with the holonomic constraint(s) satisfied using a method such as SHAKE [3], or as harmonic springs. Bend, torsion and other types of intramolecular terms are also introduced predominantly in the harmonic approximation. Intermolecular forces are approximated using two-body effective potentials, such as Coulomb interactions between point charges modelling the fixed interacting charge distributions in the system, van der Waals (dispersion) and short-range repulsive terms. The parameters of these intermolecular terms are generally determined within a mean-field approach, by tuning them to reproduce a limited set of thermodynamic data. There is no guarantee that such a force field is accurate away from the state point used to parametrise it; however, it is computationally efficient and allows long length and time scales to be reached.

2. Approximating the BO surface via quantum Drude oscillators

A richer description of the BO surface than that given by standard empirical model potentials is desirable so long as the richer model remains computationally tractable. Using QDOs to provide the BO surface, the electronic structure is not replaced by a parameterised mean-field model, but rather by a coarse-grained model involving harmonic atoms which can generate a complete description of many-body polarisation and dispersion [20–23,29]. Each harmonic atom consists of a light, negatively charged 'drudon' harmonically bonded to its corresponding positively charged nucleus. Thus, drudons are distinguishable particles obeying Boltzmann statistics. The ground-state wave function of an isolated (single) QDO has a Gaussian distribution and a large zero-point energy. A QDO thereby offers a coarse-grained Gaussian representation of the response of the electronic structure of an atom or a nearly spherical molecule to external perturbation. The reaction of this Gaussian charge distribution to external fields naturally leads to (many-body) polarisation. Quantum correlations between QDOs lead to van der Waals interactions. This includes three-body and all higher level terms in the interaction energy. There are also interactions having both characters, which are individually thought to be small in magnitude, but are numerous and complex. This complexity has been examined via the diagrammatic expansion technique for QDOs described in [23]. QDO models for large molecules can be constructed by distributing QDOs within the molecular frame (cf. [30]), similar to the way electric multipole moments are distributed to form an accurate molecular charge distribution [31].

The parameters of a QDO, mass, charge and frequency$\{m, q, \omega\}$, can be fit to reproduce the electronic responses of molecules or chemical moieties of interest, in the gas phase (polarisabilities, dispersion coefficients) [20,23], while static point charges embedded in molecular frames or chemical groups can be added to reproduce the electrostatic moments of said molecule or chemical moiety (in the gas phase) [32]. As the QDO description breaks down at short distances, short-range empirical repulsive interactions are introduced and parametrised using high-level *ab initio* computations, gas phase experimental data (scattering, viscosity, spectroscopic methods), or any useful combination thereof.

Our recent work has shown that QDOs can reproduce the long-range responses of real atoms and molecules, at least for non-reactive, closed shell species [23] including noble gases and small hydrides. The current QDO description cannot describe chemical reactions but the QDO method could be combined with *ab initio* methods in the spirit of QM/MM methods [33] or with Tersoff-type potentials [34,35], for example.

3. Path integral molecular dynamics for QDOs

The ground-state surface of the QDO model can be computed using now standard path integral molecular dynamics (PIMD) methods [36] specialised to QDOs. We call the technique the adiabatic path integral molecular dynamics for quantum Drude oscillators (APIMD-QDO). A detailed account of this method is given elsewhere [21]. Here, we outline the basic ideas, beginning with the discrete Feynman path integral formulation of statistical mechanics.

The canonical partition function $Z(\beta)$ of a quantum system is given by the trace of the density matrix operator $\hat{\rho} = e^{-\beta \hat{H}}$, where $\hat{H}$ is the system Hamiltonian and $\beta \equiv 1/k_B T$ is the inverse temperature [37]. In the position basis,

$$Z(\beta) = \mathrm{tr}\,\hat{\rho}(\beta) \;=\; \int \mathbf{d}\vec{x}\; \langle \vec{x}|\hat{\rho}(\beta)|\vec{x}\rangle \equiv \int \mathbf{d}\vec{x}\; \rho(\vec{x},\vec{x};\beta), \tag{1}$$

where $\vec{x}$ is a $3N$-dimensional configuration space position (i.e. of the drudon). The discrete Feynman path integral [38] expression for the partition function is constructed by discretising $\rho(\beta)$ into a product of P density matrices at the lower inverse temperature $\tau = \beta/P$

$$\begin{aligned}\rho(\vec{x}_0,\vec{x}_P;\beta) = \langle \vec{x}_0|e^{-\beta\hat{H}}|\vec{x}_P\rangle \;&=\; \langle \vec{x}_0|[e^{-\tau\hat{H}}]^P|\vec{x}_P\rangle \\ &= \int \mathbf{d}\vec{x}_1\mathbf{d}\vec{x}_2\ldots\mathbf{d}\vec{x}_{P-1} \\ &\quad \langle \vec{x}_0|e^{-\tau\hat{H}}|\vec{x}_1\rangle\langle \vec{x}_1|e^{-\tau\hat{H}}|\vec{x}_2\rangle\ldots \\ &\quad \langle \vec{x}_{P-1}|e^{-\tau\hat{H}}|\vec{x}_P\rangle \\ &= \int \mathbf{d}\vec{x}_1\mathbf{d}\vec{x}_2\ldots\mathbf{d}\vec{x}_{P-1} \\ &\quad \rho(\vec{x}_0,\vec{x}_1;\tau)\rho(\vec{x}_1,\vec{x}_2;\tau)\ldots\rho(\vec{x}_{P-1},\vec{x}_P;\tau)\end{aligned} \tag{2}$$

and taking the trace

$$Z(\beta) = \int \mathbf{d}^P\vec{x}\; \prod_{i=1}^{P} \rho(\vec{x}_i,\vec{x}_{i+1};\tau). \tag{3}$$

Here, $\mathbf{d}^P\vec{x} \equiv \mathbf{d}\vec{x}_1\mathbf{d}\vec{x}_2\ldots\mathbf{d}\vec{x}_P$ and $\vec{x}_{P+1} \equiv \vec{x}_1$. As written, the expression is exact for all discretisations, P. However, the new quantity τ is a small parameter which is used to motivate approximations to the exact high-temperature density matrix (or short imaginary time ($\hbar\tau$) propagator), $\rho(\vec{x},\vec{x}';\tau)$, [38,39] as discussed below.

For distinguishable particles like QDOs (and bosons, also), $\rho(\vec{x}_i,\vec{x}_{i+1};\tau)$ is positive semidefinite. Therefore, we can rewrite Equation (3) by defining an effective potential ϕ_{eff} for $N \times P$ interacting particles

$$Z(\beta) \;=\; \int \mathbf{d}^P\vec{x}\; \exp\left[-\beta\phi_{\mathrm{eff}}(\vec{x}_1,\vec{x}_2,\ldots,\vec{x}_P)\right], \tag{4}$$

where

$$\phi_{\mathrm{eff}}(\vec{x}_1,\vec{x}_2,\ldots,\vec{x}_P) \;=\; -\frac{1}{\beta}\sum_{i=1}^{P}\log\left[\rho(\vec{x}_i,\vec{x}_{i+1};\tau)\right]. \tag{5}$$

Feynman's discrete path integral formulation is thus seen to transform a quantum mechanical system of N particles into a classical system of $N \times P$ particles [38]. Later, we discuss sampling the path integral effective potential using MD techniques (note, only a canonical sampling is meaningful, here).

3.1. An approximate high-temperature density matrix

In practice, the density matrix for a complex system is not known, analytically, and approximations must be made. The most basic approach is to decompose the Hamiltonian into a reference system plus perturbation, $\hat{H} = \hat{H}_0 + \hat{V}$, and perform an operator expansion as follows [38,39]:

$$\begin{aligned}\rho(\vec{x},\vec{x}';\tau) &\equiv \langle \vec{x}|\, e^{-\tau(\hat{H}_0+\hat{V})}\,|\vec{x}'\rangle \\ &= \langle \vec{x}|\, e^{-\frac{\tau}{2}\hat{V}}\, e^{-\tau\hat{H}_0}\, e^{-\frac{\tau}{2}\hat{V}}\,|\vec{x}'\rangle + \mathcal{O}(\tau^3) \\ &= e^{-\frac{\tau}{2}V(\vec{x})}\langle \vec{x}|\, e^{-\tau\hat{H}_0}|\vec{x}'\rangle\, e^{-\frac{\tau}{2}V(\vec{x}')} + \mathcal{O}(\tau^3) \\ &= e^{-\frac{\tau}{2}V(\vec{x})}\rho_0(\vec{x},\vec{x}';\tau)\, e^{-\frac{\tau}{2}V(\vec{x}')} + \mathcal{O}(\tau^3),\end{aligned} \tag{6}$$

where it has been assumed that $\hat{V}$ is a position operator and that $\rho_0(\vec{x},\vec{x}';\tau)$ is known analytically (or easily obtained numerically by, for example, tabulation). Since QDOs are dominated by a strong on-site harmonic bond, it is natural to choose the on-site quantum harmonic oscillator Hamiltonian to be the reference system, $\hat{H}_0 = \hat{T} + (m\omega^2\hat{\vec{x}}^2)/2$, and the external potential of the interacting system of oscillators to be the potential term, $\hat{V} = \hat{V}_{\mathrm{ext}}$. The harmonic oscillator density matrix is known in closed form [38] and, for an N particle system, can be written as

$$\begin{aligned}\rho_0(\vec{x},\vec{x}';\tau) = \left[\frac{\alpha_P(\beta)}{\pi}\right]^{3N/2} \exp\Bigg[&\alpha_P(\beta)(\vec{x}-\vec{x}')^2 \\ &+ \frac{\lambda_P(\beta)}{2}(\vec{x}^2+(\vec{x}')^2)\Bigg],\end{aligned} \tag{7}$$

where

$$\alpha_P(\beta) = \frac{m\omega}{2\hbar \sinh(f)},$$
$$\lambda_P(\beta) = \frac{2m\omega \tanh\left(\frac{f}{2}\right)}{\hbar},$$
$$f = \frac{\beta\hbar\omega}{P} = \tau\hbar\omega. \tag{8}$$

The above expression reduces to the usual free particle reference in the limit $\tau\hbar\omega \to 0$ wherein $\alpha_P(\beta) \to m/(2\hbar^2\tau)$ and $\lambda_P(\beta) \to \tau m\omega^2/2$. Above, it is assumed that the origin of each of the $\vec{x}_i = \{\mathbf{x}_{1,i} \ldots \mathbf{x}_{N,i}\}$ is pinned to the molecular site to which it is assigned, $\vec{X} = \{\mathbf{X}_1 \ldots \mathbf{X}_N\}$ (i.e. the corresponding Drude nucleus).

We can now define the approximate partition function for an N particle QDO system as

$$Z_P(\beta) = \int \mathbf{d}^P\vec{x} \left[\prod_{i=1}^{P} \rho_0(\vec{x}_i, \vec{x}_{i+1}; \tau)\right] \times \exp\left(-\tau \sum_{i=1}^{P} V_{\text{ext}}(\vec{x}_i)\right) = Z(\beta) + \mathcal{O}(P\tau^3), \tag{9}$$

which we shall endeavour to sample in the next subsection.

3.2. *Sampling*

3.2.1. *Harmonic staging form of the density matrix*

In order to sample $Z_P(\beta)$ efficiently for the N-body QDO problem, it is instructive to note that $\rho_0(\vec{x}_i, \vec{x}_{i+1}; \tau)$ introduces a strong nearest neighbour coupling between beads or imaginary time slices i and $i+1$ for each QDO drudon. That is, bead i of particle k interacts with bead $i+1$ of particle k via a strong harmonic term and with its tether site (nucleus) by another strong harmonic term. Given that the system is highly quantum mechanical, these two terms dominate the effective potential which must be sampled. It is therefore useful to employ the following algebraic identity [21,36,40,41] to yield

$$\prod_{i=1}^{P} \rho_0(\vec{x}_i, \vec{x}_{i+1}; \tau) = \rho_0(\vec{x}_1, \vec{x}_1; \beta)\left[\prod_{i=2}^{P} \frac{\rho_0(\vec{x}_1, \vec{x}_i; (i-1)\tau)\rho_0(\vec{x}_i, \vec{x}_{i+1}; \tau)}{\rho_0(\vec{x}_1, \vec{x}_{i+1}; j\tau)}\right], \tag{10}$$

where $\vec{x}_1 = \vec{x}_{P+1}$ as above. For Gaussian density matrices, the identity takes the form

$$\prod_{i=1}^{P} \rho_0(\vec{x}_i, \vec{x}_{i+1}; \tau) = \left[\prod_{i=1}^{P} \left(\frac{1}{2\pi\sigma_i^2}\right)^{3N/2} \exp\left(-\frac{\vec{u}_i^2}{2\sigma_i^2}\right)\right], \tag{11}$$

where

$$\vec{u}_1 = \vec{x}_1,$$
$$\vec{u}_i = \vec{x}_i - \vec{x}_i^*. \tag{12}$$

For the special case of the quantum harmonic oscillator,

$$\vec{x}_i^* = \frac{\sinh(\tau\hbar\omega)}{\sinh[i\tau\hbar\omega]}\vec{x}_1 + \frac{\sinh[(i-1)\tau\hbar\omega]}{\sinh[i\tau\hbar\omega]}\vec{x}_{i+1}, \tag{13}$$
$$\sigma_i^2 = \frac{\hbar \sinh[(i-1)\tau\hbar\omega]\sinh(\tau\hbar\omega)}{m\omega \sinh[i\tau\hbar\omega]}$$

for $i = 2, \ldots, P$ and

$$\sigma_1^2 = \frac{\hbar}{2m\omega \tanh\left(\frac{\beta\hbar\omega}{2}\right)}. \tag{14}$$

The new variables, $\vec{u}$, can be used as a linear transform which diagonalises the reference harmonic density matrix. The transformation has a unit Jacobian and hence the partition function can be written as

$$Z_P(\beta) = \int \mathbf{d}^P\vec{u} \left[\prod_{i=1}^{P} \left(\frac{1}{2\pi\sigma_i^2}\right)^{3N/2} \exp\left(-\frac{\vec{u}_i^2}{2\sigma_i^2}\right)\right] \times \exp\left(-\tau \sum_{i=1}^{P} V_{\text{ext}}(\vec{x}_i(\vec{u}))\right). \tag{15}$$

We note the transformation between $\vec{x}$ and $\vec{u}$ given by Equations (12) and (13) and its inverse,

$$\vec{x}_i = \vec{u}_i + \frac{\sinh[(i-1)\tau\hbar\omega]}{\sinh[i\tau\hbar\omega]}\vec{x}_{i+1} + \frac{\sinh[\tau\hbar\omega]}{\sinh[i\tau\hbar\omega]}\vec{x}_1, = \sum_{l=i}^{N+1} \frac{\sinh[(i-1)\tau\hbar\omega]}{\sinh[(l-1)\tau\hbar\omega]} u_l + A_i u_1, \tag{16}$$

where

$$A_{N+1} = 0,$$
$$A_i = \frac{\sinh[(i-1)\tau\hbar\omega]}{\sinh[i\tau\hbar\omega]} A_{i+1} + \frac{\sinh[\tau\hbar\omega]}{\sinh[i\tau\hbar\omega]}, \tag{17}$$

can be computed with linear complexity in P [21,36].

3.2.2. Staging path integral molecular dynamics

In order to generate an effective MD method, it is natural to work in the $\vec{u}$ staging coordinate system and introduce momenta conjugate to these variables. In the canonical ensemble, this is accomplished by inserting a set of Gaussian integrals as these can be performed analytically and the result cancelled by a multiplicative constant [21,36,42]

$$Z_P(\beta) = C \int \mathbf{d}^P \vec{p} \int \mathbf{d}^P \vec{u} \left[\prod_{i=1}^{P} \left(\frac{1}{2\pi\sigma_i^2} \right)^{3N/2} \times \exp\left(-\frac{\vec{u}_i^2}{2\sigma_i^2} \right) \right] \exp\left(-\tau \sum_{i=1}^{P} V_{\text{ext}}(\vec{x}_i(\vec{u})) \right) \times \exp\left(-\beta \sum_{i=1}^{P} \frac{\vec{p}^2}{2\tilde{m}_i} \right) \tag{18}$$

$$C = \prod_{i=1}^{P} \left[\frac{\beta}{2\pi\tilde{m}_i} \right]^{3N/2}.$$

The result defines a faux classical Hamiltonian

$$H^{(\text{faux})} = \sum_{i=1}^{P} \frac{\vec{p}^2}{2\tilde{m}_i} + \frac{\vec{u}_i^2}{2\sigma_i^2\beta} + \frac{V_{\text{ext}}(\vec{x}_i(\vec{u}))}{P}, \tag{19}$$

which can be used to sample the path integral via *canonical* MD methods as only the canonical ensemble is meaningful, here (the canonical dynamics method selected *must* be ergodic or nearly so for harmonic systems). A good choice of faux mass set $\{\tilde{m}\}$ is

$$\tilde{m}_i = \frac{1}{(\gamma\tilde{\omega}\sigma_i)^2} \tag{20}$$

which equalises the harmonic staging mode motions to move on the desired time scale, $1/(\gamma\tilde{\omega})$. The choice of γ and $\tilde{\omega}$ will be described below when nuclear motion is introduced.

3.2.3. Faux high electronic temperature

Since systems of QDOs represent a coarse-grained electronic structure, they have a large ground-state energy ($\approx 3N\hbar\omega/2$) and a first excitation energy of $\approx\hbar\omega/k_B$ on the order of 10^5 K. The discretisation scheme of Equation (6) will not be sufficient for the strength of external potentials of interest in the QDO context, unless $\tau\hbar\omega < 1$. Therefore, a straightforward APIMD-QDO treatment would require thousands of beads at ambient temperature. Although the computational cost of APIMD-QDO increases linearly with bead number P, this is a nonetheless a prohibitively large value.

We note that QDOs remain dominated by the ground state at temperatures as high as 30 times ambient. This observation motivates us to simulate the QDO representation of the *electronic* degrees of freedom at a temperature 30 times greater than the thermodynamic (i.e. atomic or nuclear) temperature of interest. The faux high temperature, T_{QDO} or small imaginary time, $\hbar\beta_{\text{QDO}}$, allows smaller bead numbers to be employed with a little effect on the resulting BO surface. Typically, $\hbar\beta_{\text{QDO}} = 10/\omega$ is sufficient. However, as discussed in the next subsection, the use of $T_{\text{QDO}} > T$ comes at the price of the introduction of an adiabatic principle.

3.2.4. Time scale separation and nuclear motion

In order to evolve the nuclei on the ground-state surface given by the $3N \times P$ 'hot' drudon path integral bead degrees of freedom, it is necessary to ensure that the drudon bead motion is fast relative to the nuclear motion. This separation of time scales imposed by the use of an elevated electronic temperature (T_{QDO}) allows the sampling of the path integral to converge sufficiently well so as to generate a correct average force on the nuclei. In the absence of the elevated electronic temperature, a correct sampling of statistical averages would result without a time scale separation. Canonical MD methods (ergodic or nearly so for the harmonic oscillator) which deal with a separation of temperatures are known [43] and recent developments [44] can help improve performance.

We accomplish the time scale separation, in practice, by scaling down the masses in the staging basis until static properties of the system converge (see Figure 4 and later discussion). This is controlled by the parameters $\gamma\tilde{\omega}$. We take $\tilde{\omega} = 0.05/\Delta t_{\text{MD}}$ where Δt_{MD} is the time step required to integrate a comparable standard MD simulation; that is a single harmonic oscillator of said frequency ($\tilde{\omega}$) can be integrated accurately using a time step of Δt_{MD} ($\tilde{\omega}\Delta t_{\text{MD}} = 0.05$). The parameter γ indicates how much faster the drudon-beads are moving in comparison to the atoms; it increases the harmonic bead motion frequencies by a factor of γ. The APIMD-QDO integration time step is, thus, $\Delta t_{\text{MD}}/\gamma$.

It is now useful to consider the computational efficiency of the APIMD-QDO method. The product of bead number $P \approx 90$ and the 'adiabaticity factor' $\gamma \approx 16$ (see below) represents the overhead of performing APIMD-QDO relative to MD. However, P can be parallelised well on modern architectures [45,46]. Consider the concrete example of water. A rigid water model may be integrated using a time step of 2.4 fs under standard MD, while QDO water requires a time step of $\Delta t = 0.15$ fs, comparable to that employed in Car-Parrinello *ab initio* MD (CPAIMD) simulations [15]. The *advantage* of APIMD-QDO over CPAIMD is that although APIMD-QDO gives rise to a coarse-grained electronic structure which includes high-level correlation effects, the method scales linearly with the number of particles, N, (or $N \log N$ in the periodic systems with the long-range interactions treated using particle mesh Ewald methods [47,48]), permitting large systems to be studied. The

comparative disadvantage of APIMD-QDO is that the technique does not allow bond making and breaking although QDOs could be implemented in the context of a Tersoff-type model [34,35] or combined with *ab initio* techniques in a QM/MM approach [33], for example.

3.3. *Energy estimators*

It is well known in the computational path integral literature [21,42,49] that low variance energy estimators are key to obtaining accurate results. This is problematic for the QDO model which has a large, non-zero vacuum energy (i.e. the energy when $\hat{V}_{\rm ext} = 0$) as was addressed in [21]. The large vacuum energy arises from the fact that the QDOs represent an electronic structure whose fundamental frequency (ω) is high.

Briefly, in order to calculate thermodynamic observables, we start with the partition function and take appropriate derivatives [37]. For the energy, its average with respect to the quantum ensemble for a discrete path integral treatment with an approximate high-temperature propagators is written as

$$E_P = -\frac{\partial}{\partial\beta}\ln Z_P(\beta) \qquad (21)$$
$$= \int \mathbf{d}^P\vec{x}_j \left(\frac{\partial(\beta\phi_{\rm eff})}{\partial\beta}\right)\frac{e^{-\beta\phi_{\rm eff}}}{Z(\beta)} \equiv \left\langle\frac{\partial(\beta\phi_{\rm eff})}{\partial\beta}\right\rangle,$$

where the last average is over the classical ensemble defined by $\phi_{\rm eff}$.

Equation (21) is known to have a large variance [21,49] making convergence of statistical averages slow in any sampling scheme. As discussed above, the problem is exacerbated for the QDO model by the large energy of the unperturbed harmonic oscillator, $E_0 = \frac{3N\hbar\omega}{2}\coth(\beta\hbar\omega/2) \approx \frac{3N\hbar\omega}{2}$ for $\beta\hbar\omega \geq 10$. In [21], an *exact equivalent* with low variance was derived

$$E_P = E_{P,hsv} = \frac{3N\hbar\omega}{2}\coth\left(\frac{\beta\hbar\omega}{2}\right)$$
$$-\frac{\tau\hbar\omega}{2P}\coth\left(\frac{\beta\hbar\omega}{2}\right)\left\langle\sum_{i=1}^{P}\sum_{j=1}^{P}\vec{x}_j D_{i-j+1}\vec{\nabla}_i V_{\rm ext}(\vec{x}_i)\right\rangle$$
$$+\frac{\tau\hbar\omega}{2P}\coth(\tau\hbar\omega)\left\langle\sum_{i=1}^{P}\vec{x}_i\vec{\nabla}_i V_{\rm ext}(\vec{x}_i)\right\rangle$$
$$+\frac{1}{P}\left\langle\sum_{i=1}^{P}V_{\rm ext}(\vec{x}_i)\right\rangle. \qquad (22)$$

Here, because the energy of the unperturbed system ($V_{\rm ext} \to 0$) is given exactly (in the first term), the harmonic staging virial (*hsv*) estimator was shown improve convergence of the statistical sampling of the energy [21]. The coefficients D embody correlations along the chain and are given by

$$D_1 = 1, \qquad D_i = A_i + \frac{\sinh[(i-1)\tau\hbar\omega]}{\sinh[\beta\hbar\omega]}, \qquad (23)$$

where the A_i are defined above. Note the double sum over P in the *hsv* estimator is a convolution which can be computed in $N(P\ln P)$ complexity [21] as $\{D\}$ is periodic in P. A low variance estimator for the pressure is given in [21].

4. Simulation studies of the Mark 1.0 QDO water model

In this section, we will review our recently developed Mark 1.0 QDO model for water [29] and test its transferability to the liquid–vapour interface. Studies using the Mark 2.0 model that exhibits improved thermodynamic properties due to the development of refined short-range repulsive interactions are currently underway.

We have chosen to use the rigid TIP4P geometry [50] as the basis for our QDO water model [29] (see Figure 1). Fixed positive charges (of the same value by symmetry) are placed on the two hydrogen sites, while a third, neutralising negative charge is placed on the HOH angle bisector at a site referred to as 'M'. The position of the M site and the charges are selected to reproduce the dipole moment of the isolated molecule exactly and minimise the least-squares difference between the model and the measured values for the components of the quadrupole moment. A single QDO is placed on the M site as the polarisability tensor of a water molecule is nearly isotropic. The QDO parameters

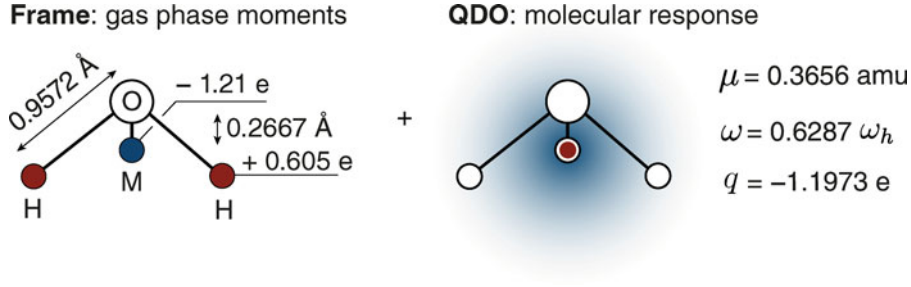

Figure 1. A representation of the electrostatics of QDO water [29]. $\omega_h = E_h/\hbar$ is the Hartree frequency.

were selected to reproduce the spherical component of the monomer's polarisabilities and dispersion coefficients. The empirical repulsion potential between the O sites is taken to be isotropic (the sum of two exponentials) [23]. The nuclear motion of our rigid model is studied in the classical limit using SHAKE [3] to hold the molecular frame rigid. The results presented here are generated using the Mark 1.0 model that nonetheless gives a qualitative description of bulk water and thereby demonstrates the applicability of the APIMD-QDO method to a complex molecular system [29].

We have simulated the liquid–vapour interface predicted by the Mark 1.0 QDO water using $N = 300$ molecules in an orthorhombic unit cell of dimension $20.8 \times 20.8 \times 80\,\text{Å}^3$, with periodic boundary conditions at $T = 300$ K. Long-range interactions were computed via Ewald summation [51,52]. To generate initial conditions, an equilibrated van der Waals liquid at experimental density ($1\ \text{g cm}^{-3}$) was decorated with hydrogen atoms to create water molecules. The resulting configuration was equilibrated using TIP4P in a cubic unit cell $20.8 \times 20.8 \times 20.8\,\text{Å}^3$. After the initial equilibration, the z-dimension of the simulation box was expanded to 80 Å and the liquid was equilibrated using the standard TIP4P model to create the interface. Finally, the resulting configuration was equilibrated using QDO water. The results presented in Section 4.3 were obtained as averages over a further 250 ps.

4.1. *Error control in APIMD-QDO simulations of water*

In APIMD-QDO, there are several sources of systematic error. The finite number of beads, P, the finite integration time step, Δt and the time scale separation factor required to achieve adiabatic nuclear motion, γ. All contribute to errors in calculated thermodynamic and structural properties. In order to estimate the errors introduced by these factors we have performed a series of APIMD-QDO calculations on bulk water with a systematic variation of each factor. The convergence of the pressure, p, is used as an estimate of the error. The computations were performed at the state point $\{T = 300\ \text{K}, \rho = 1\ \text{g cm}^{-3}\}$ using $N = 300$ molecules, periodic boundary conditions and, as above, Ewald summation [51,52] to compute the long-range interactions.

Figure 2 shows the dependence of pressure, p, on the number of beads, P. Linear extrapolation of $p \sim p(0) + \epsilon_P P^{-2}$ to $P^{-2} \to 0$ gives $p(0) = 5.4$ kbar at the experimental density. Figure 2 also shows that $P = 96$ beads are sufficient to achieve good convergence. Since the repulsion in the Mark 1.0 model is unoptimised, the equilibrium density is underestimated leading to a residual pressure at the experimental density. We note that as is usual in path integral computations, the classical limit is overbound resulting in a negative pressure at small bead numbers. The asymptotic

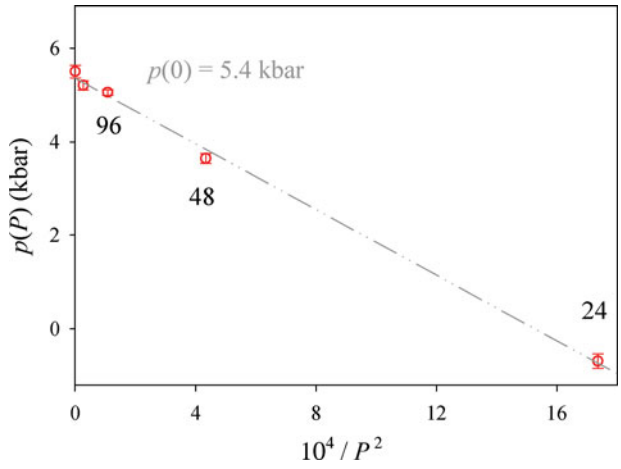

Figure 2. The convergence of the pressure with respect to the number of beads. We take 96 beads to be sufficient.

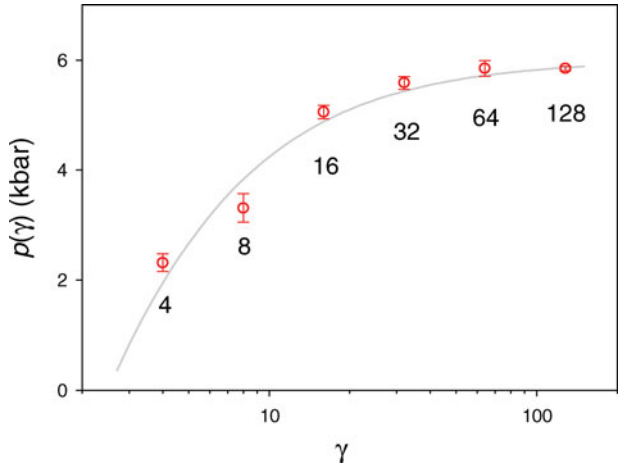

Figure 3. The convergence of the pressure with respect to the time scale separation parameter γ. Based on the results, we have adopted $\gamma = 16$.

value of the polarisability is independent of the number of beads (as it is a classical quantity), but its short-range damping behaviour is not nor are the dispersion coefficient values.

The pressure is also affected by the APIMD-QDO adiabatic separation given by γ, as illustrated in Figure 3. The results exhibit a plateau below $\Delta t = 0.15$ fs, which we take as our baseline (i.e. $\gamma = 16$ and $\Delta t = \Delta t_{\text{MD}}/\gamma = 0.15$ fs).

Lastly, the effect of varying the integration time step, Δt, at fixed γ on the simulation results is studied; the convergence of the pressure as a function of time step is given in Figure 4. The results indicate that $\Delta t = 0.15$ fs at $\gamma = 16$ is sufficient, validating the assumption that taking $\tilde{\omega}\Delta t_{\text{MD}} = 0.05$ allows the path integral beads to be integrated accurately. The multiple time step strategy employed is given below.

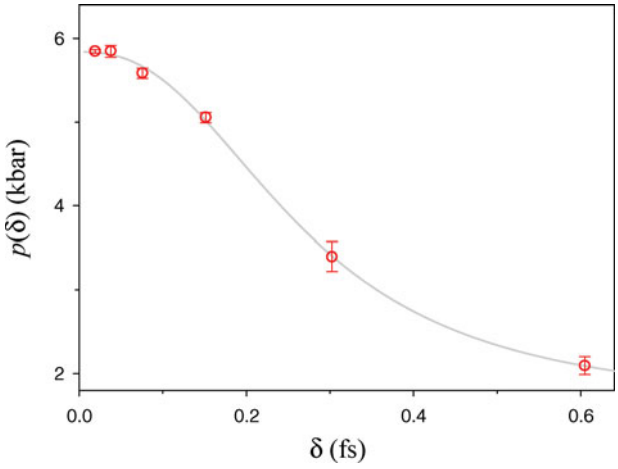

Figure 4. The convergence of the pressure with respect to the APIMD-QDO integration time step with $\gamma = 16$ fixed. Based on these results, we have adopted $\Delta t = 0.15$ fs. In these and all computations presented herein, $n = 5$ multiple time steps are used to integrate the fast staging modes.

4.2. *Performance of the current implementation – QDrude-Sim*

We have developed a stand-alone QDO-based application called QDrude-Sim which performs diffusion Monte Carlo simulations [53] of clusters and periodic systems with heavy atoms fixed following the methods of [22] and APIMD-QDO simulations of clusters and periodic systems including heavy atom motion as described above [21]. For the APIMD-QDO simulation, the beads were parallelised following [45,46] and the N atoms of each imaginary time slice (bead) parallelised according to the most basic method described in [54] (data replication). The multiple time step integration scheme used follows [36,45,55–57]; one multiple time step level was employed (unperturbed harmonic staging interactions) with $n = 5$ small time steps of size $\Delta t/n$ was applied in all computations presented herein.

In order to demonstrate the capabilities of QDrude-Sim, we present the performance of the application on simulation studies of bulk liquid water using the protocols established in the previous subsection. The code scales approximately linearly with system size as shown in Figure 5(a). It parallelises water well somewhat beyond $P = N_{\text{proc}}$ due to the simple scheme used to treat the atoms (see Figure 5(b)). We are currently working to improve the performance and applicability of the software.

4.3. *Results – Mark 1.0 QDO water model liquid–vapour interface*

Figure 6 shows the variation of the molecular density and the mean molecular dipole moment through the liquid–vapour interface. In order to improve the statistics, the data from the two interfaces in the slab were symmetrised. The

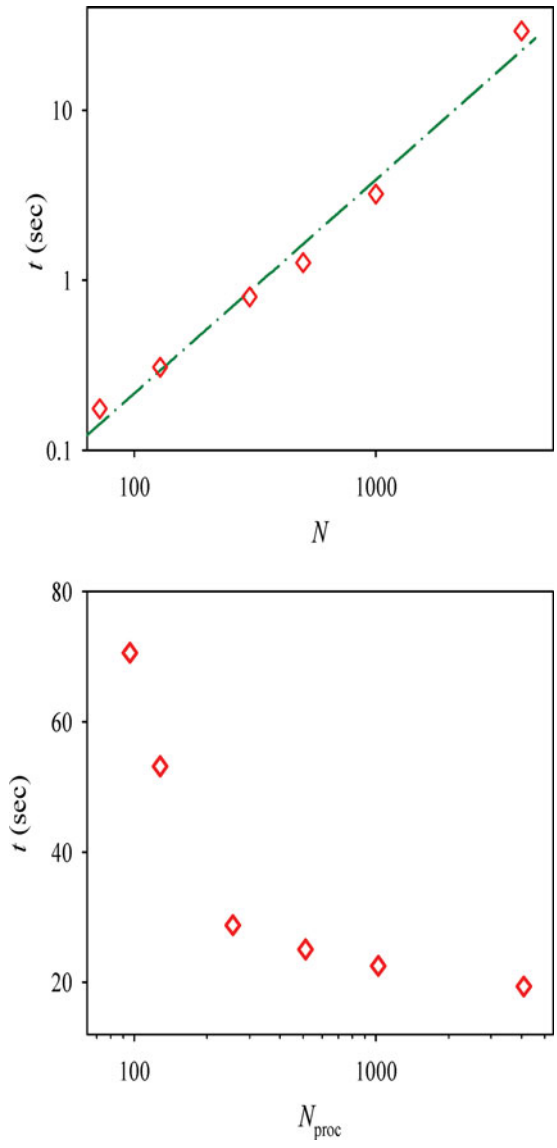

Figure 5. (colour online). (a) QDrude-Sim timings for $N = 72$, 128, 300, 500, 1000 and 4000 water molecules computed with $P = 96$ beads and a $\Delta t = 0.15$ fs time step. (b) Parallel scaling of a $N = 4000$ water molecule system computed with $P = 96$ beads and a $\Delta t = 0.15$ fs time step. The calculations were performed on IBM Blue Gene/Q 'blue joule' at the STFC Hartree Centre at Daresbury Laboratory.

density profile is flat within the slab, and approximately zero outside it, as expected. The dipole moment convergences to the value observed for the Mark 1.0 QDO water model bulk, $\mu = 2.6$ D [23], at a penetration of only a couple of molecular widths into the surface. However, the surface layer shows a significant dipole reduction that will affect the physics of the surface. For the few molecules that evaporate from the liquid, the dipole moment remains close to $\mu = 1.855$ D, the experimental value for the gas phase.

Figure 7 shows in more detail how the charge distribution of individual molecules changes throughout the slab,

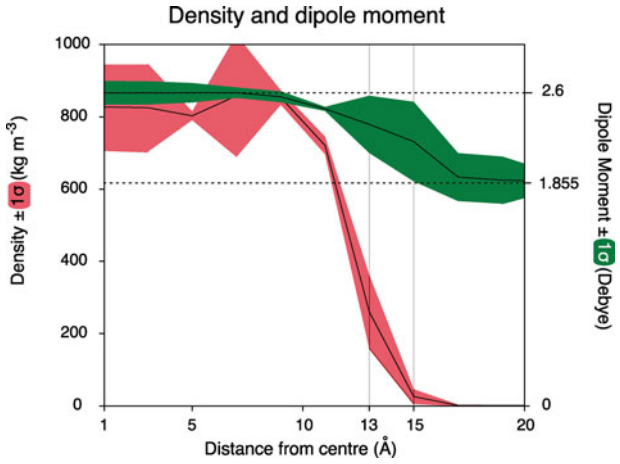

Figure 6. (colour online). The mass density and average dipole moment for the slab of water, averaged over slices of the slab, as a function of distance normal to the surface from the centre of the slab. Note the density within the slab is ≈850 kg m^{-3} rather than ≈1000 kg m^{-3} because the Mark 1.0 model employed here is unoptimised. Note that the dipole moment is significant in gas phase (1.855 D) and also exhibits a significant enhancement in condensed phase (2.6 D). The dipole enhancement changes continuously across the interface, an effect not reproduced by fixed-charge models. Note also that it falls off more slowly than the density. This means that molecules that are on the outside surface of the slab nevertheless experience substantial polarisation effects, yielding a dipole enhancement that is different from both the bulk liquid and the gas.

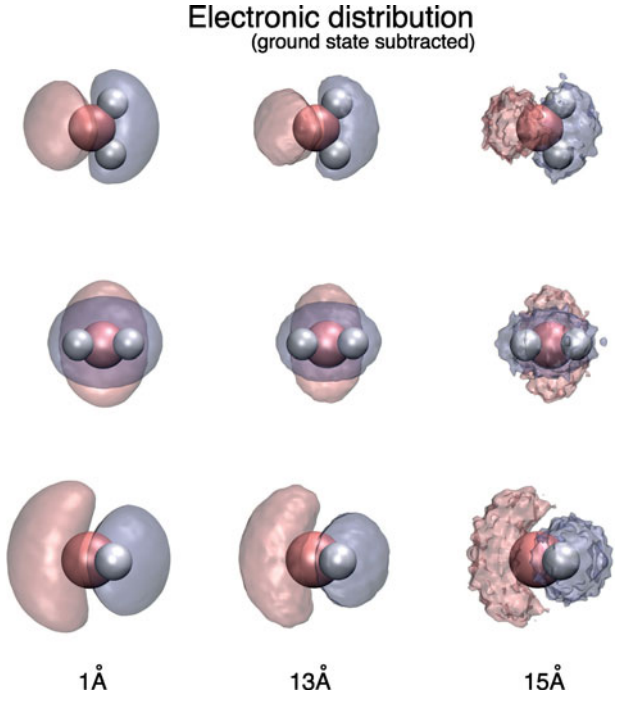

Figure 7. (colour online). The detailed average electronic polarisation relative to the unperturbed gas-phase or isolated monomer, for the QDO model water molecule at various stages of the transition from the bulk out through the surface (left to right) of a slab of water at $T = 300$ K, represented by losses (blue) and gains (pink) of electronic density. In the liquid (first and second images) the observed pattern reflects the tetrahedral structure present in liquid water; electronic density is lost (blue) from around outgoing hydrogen bonds and gained (pink) around incoming hydrogen bonds, yielding a significant enhancement of the molecular dipole, by 40%, but also enhancement of the molecular quadrupole. On the outside surface of the liquid (second image) the shape of the polarisation pattern remains roughly the same but the magnitude decreases considerably. This is because polarisation is a many-body effect and for a molecule on the surface, half or more of its first-shell neighbours will be missing, compared with a molecule in the bulk. Finally, away from the surface (third image) the structure is completely lost. In this last image, there is an increasing amount of sampling noise. This is due to the scarcity of molecules in a given volume of a gas. These distributions were generated by averaging over many molecular configurations from simulation, sampling Drude density by projecting bead positions onto the molecular frame, binning into a three-dimensional array, and then subtracting the exactly known unperturbed density distribution of the isolated monomer, $\rho(x) = \sqrt{\frac{m\omega}{\pi\hbar}} \exp\left(-\frac{m\omega}{\hbar}x^2\right)$.

information available because the QDO model generates a coarse-grained electronic structure. The isosurfaces show the perturbation of the QDO's electronic distribution from that of the ideal isolated monomer, for water molecules in the bulk and surface regions. There is a strong dipole enhancement as charge shifts along the bisector of the molecule. There is also a tetrahedral character to the shift, reflecting the arrangement which water molecules take in the condensed phase. The electronic charge shifts towards the positive hydrogen atoms of neighbouring molecules forming incoming hydrogen bonds, and thus is displaced from its own hydrogen atoms, which form outgoing hydrogen bonds. This redistribution creates a strong enhancement of the dipole moment in the x-direction (bisector of the molecule), a strong enhancement of the quadrupole's yy component (H-H direction) and a similar reduction of the quadrupole's zz component (out of plane). These detailed polarisation effects are beyond what can be captured by point-polarisable models or by fluctuating charge models of water, the latter of which polarise only in the plane of the molecule. Higher order polarisation (beyond dipole) can play a significant role in water physics. For example, the ability of empirical models to reproduce the phase diagram of water has been found to depend on the ratio of the molecular dipole to the molecular quadrupole [58].

In order to gain a quantitative picture of the density variation, we fit the density to the following function:

$$\rho(z) = \frac{\rho_0}{2}\left[1 + \tanh\left(\frac{(z_g - z)}{\delta}\right)\right] \tag{24}$$

giving

$$\rho_0 = (820 \pm 10)\,\text{kg m}^{-3}, \quad z_g = (12.5 \pm 0.2)\,\text{Å},$$
$$\delta = (1.42 \pm 0.2)\,\text{Å}.$$

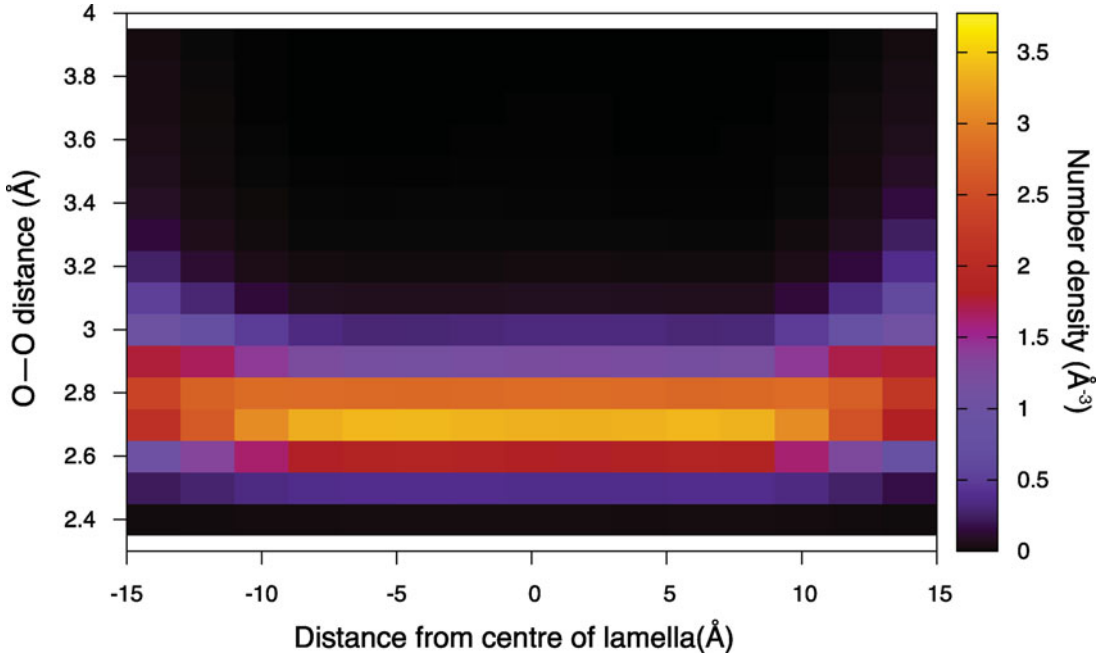

Figure 8. (colour online). The number density of first neighbours with a particular O–O distance from a molecule as a function of the distance from the centre of the slab. For molecule in the surface region, this number density is skewed towards higher values, indicating an expansion of the O–O distance in the surface region.

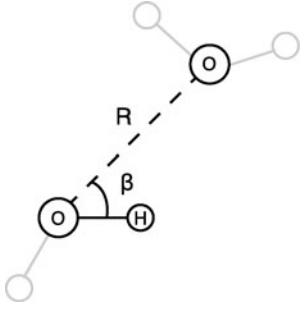

Figure 9. Geometry between two neighbouring water molecules used to calculate the potential of mean force (PMF) between them.

We find a bulk density about 20% smaller than the experimental. This is a consequence of the fact that we used an unoptimised model, here. We have recently fit a QDO model with the correct density at room temperature and pressure (the Mark 2.0).

We define the surface as the region where the density drops from 90% to 10%, giving a surface thickness of $\Delta z = (3.1 \pm 0.4)$ Å. This thickness is comparable to the van der Waals diameter of a water molecule, showing that the surface is roughly a single molecule thick. This observation is consistent with both classical simulations (TIP4P-POL2 [59] reporting $\Delta z = 3.92$ Å [60]) and a recent *ab inito* study reporting $\Delta z = 3.76$ Å [61].

In order to investigate the structure of the surface in more detail, we calculated the average oxygen–oxygen distance R_{OO} between nearest-neighbour molecules. In this context, nearest-neighbour means 'the closest molecule with respect to a reference molecule'. At the surface, defined as previously, $R_{OO}^{(s)} = (2.799 \pm 0.002)$ Å. We also calculated this distance in the bulk liquid, using an equilibrated NPT (constant particle number, N, pressure, P, and temperature, T, ensemble) sample and averaging over 70 ps, obtaining $R_{OO}^{(b)} = (2.728 \pm 0.003)$ Å. Our results show an elongation of the average oxygen–oxygen distance by about 2.6% at the liquid–vapour interface. This result is consistent with the latest *ab inito* studies [61] of the surface, which report an elongation of around 1%. Experiment predicts an elongation as well, as high as 6% [62]. In this aspect, QDO-water and Dang–Chang model water [63] (the latter of which predicts a smaller elongation of 0.5% [61]) are unique among empirical models, most of which (including TIP4P-POL2 [59]) predict a reduction of the oxygen–oxygen distance at the surface [60]. The elongation of the oxygen–oxygen distance at the surface of QDO water shows that accurate electronic response is necessary in reproducing the physics of heterogeneous interfaces.

This elongation is also stable with respect to the definition of a nearest neighbour. Both averaging the O–O distance with respect to all neighbours in a shell of radius 3.5 Å and with respect to all hydrogen bonded neighbours gives an elongation of around 1%.

To investigate the surface elongation effect in more detail, Figure 8 shows the probability density of a given oxygen–oxygen distance as a function of distance from

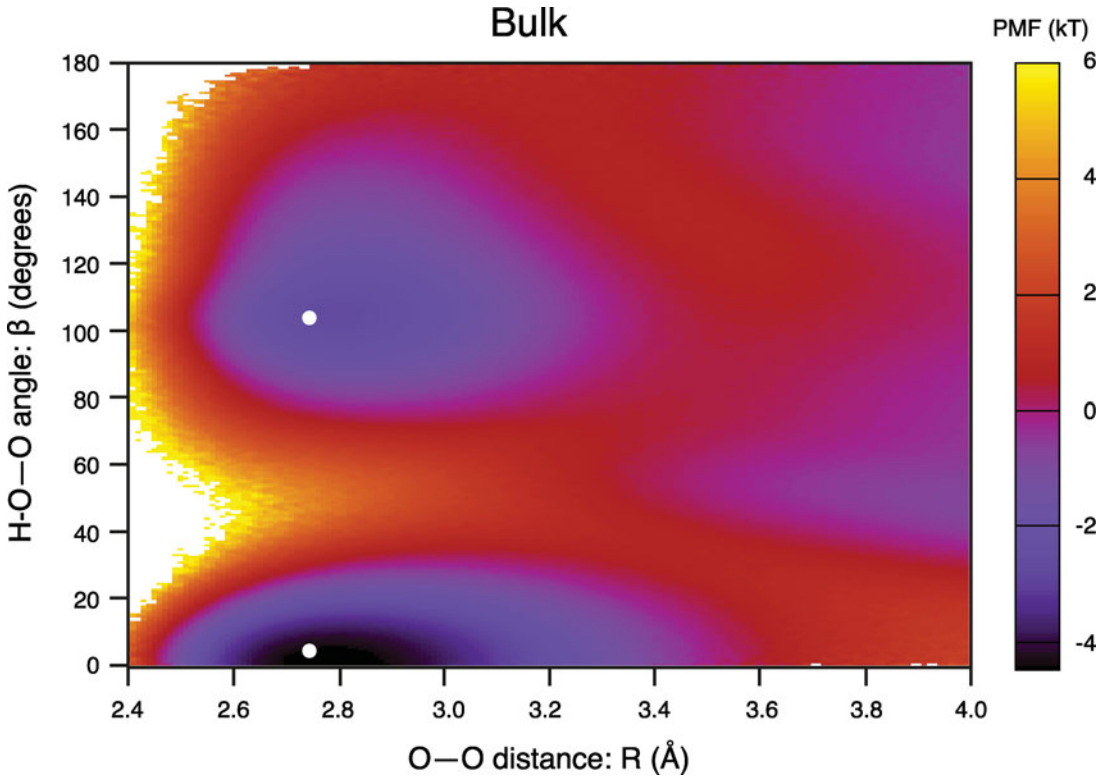

Figure 10. (colour online). The potential of mean force (PMF) between two neighbouring molecules in the bulk region of the slab. See Figure 9 for the considered geometry. The white dots are a guide to the eye and are plotted at 2.73 Å, the average O–O distance between two bulk molecules.

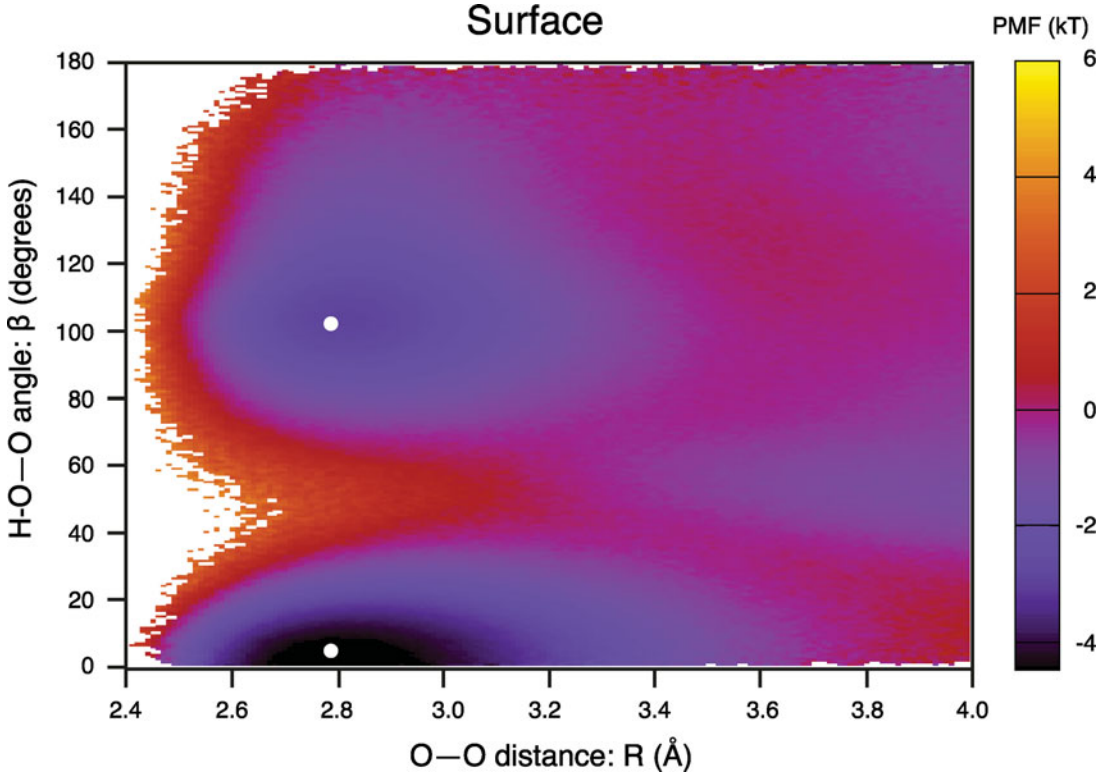

Figure 11. (colour online). The potential of mean force (PMF) between two neighbouring water molecules in the surface region of the slab. See Figure 9 for the definition of the distance and angle. The white dots are a guide to the eye and are plotted at 2.80 Å, the average O–O distance between two surface molecules.

the centre of the simulation box. At both the positive and negative z surfaces of the slab, the probability distribution shows a long tail towards higher O–O distances, resulting in the elongation previously described.

This surface elongation has its roots in the changing character of the hydrogen bonds at the surface. To understand this behaviour, we generated the distribution function $g(R, \beta)$ in the two regions (here R is the oxygen–oxygen distance between two molecules and β is the O–H–O angle as depicted in Figure 9). Figures 10 and 11 show the corresponding potentials of mean force (PMFs) computed from the distribution functions, $\mathrm{PMF}(R, \beta) = -k_\mathrm{B}T \ln(g(R, \beta))$. Hydrogen bonds are formed in the valleys of the PMF and show a similar character in both the bulk and surface regions. At the surface, there is an elongation of both the accessible O–O distance and angular range, resulting in 'looser' hydrogen bonds.

5. Summary and conclusions

A path-integral-based method, APIMD-QDO, capable of applying the QDO model of intermolecular forces, which gives a consistent treatment of many-body polarisation and dispersion [23], to molecular systems, is described. The computational complexity of the APIMD-QDO technique scales linearly with system size and has low overhead on modern computer architectures. Thus, the QDO's Gaussian coarse-grained electronic structure can be used to provide an accurate BO surface for classical MD simulations of the structure of matter in many contexts. The application presented here, water's liquid–vapour interface, demonstrates the applicability of the QDO's Gaussian coarse-grained electronic structure to a non-trivial, complex interfacial system. We have presented here early results generated using the Mark 1.0 QDO water model [29]; more realistic parameter values have been determined and results are now being generated for the Mark 2.0 model which exhibits improved thermodynamic properties.

Acknowledgements

This work was supported in part by the National Physical Laboratory Strategic Research Programme and IBM Research. We acknowledge use of STFC Hartree Centre resources funded by the UK's investment in e-Infrastructure. This work (A.P. Jones) has been supported in part by the European Metrology Research Programme (EMRP). G.J. Martyna acknowledges an Honourary Professorship in the School of Physics and Astronomy at the University of Edinburgh.

References

[1] A. Rahman, Phys. Rev. **136**, A405 (1964).
[2] L. Verlet, Phys. Rev. **159**, 98 (1967).
[3] J.P. Ryckaert, G. Ciccotti, and H.J.C. Berendsen, J. Comp. Phys. **23**, 327 (1997).
[4] M. Allen and D. Tildesley, *Computer Simulations of Liquids* (Claredon Press, Oxford, UK, 1989).
[5] J. Hansen and I. McDonald, *Theory of Simple Liquids* (Accademic Press, New York, 1986).
[6] M. Wilson, P. Madden, M. Hemmati, and C. Angell, Phys. Rev. Lett. **77**, 4023 (1996).
[7] J. Antony, J. Piquemal, and N.J. Gresh, J. Comp. Chem. **26**, 1131 (2005).
[8] W. Cochran, Phil. Mag. **4**, 1082 (1959).
[9] B.G. Dick and A.W. Overhauser, Phys. Rev. **112**, 90 (1958).
[10] M. Sangster and M. Dixon, Adv. Phys. **3**, 247 (1976).
[11] G. Lamoureux, A.D. MacKerell, and B. Roux, J. Chem. Phys. **119**, 5185 (2003).
[12] C.J. Burnham and S.S. Xantheas, J. Chem. Phys. **116**, 1479 (2002).
[13] P. Hohenberg and W. Kohn, Phys. Rev. **136**, B864 (1964).
[14] W. Kohn and L. Sham, Phys. Rev. **140**, A1133 (1965).
[15] R. Car and M. Parrinello, Phys. Rev. Lett. **55**, 2471 (1985).
[16] S. Grimme, Wiley Interdiscip. Rev. Comput. Mol. Sci. **1**, 211 (2011).
[17] A. Donchev, Chem. Phys. **125**, 074713 (2006).
[18] M. Cole, D. Velegol, H.Y. Kim, and A. Lucas, Mol. Simul. **35**, 849 (2009).
[19] Y. Shtogun and L. Woods, J. Phys. Chem. Lett. **1**, 1356 (2010).
[20] T.W. Whitfield and G.J. Martyna, Chem. Phys. Lett. **424**, 409 (2006).
[21] T. Whitfield and G.J. Martyna, J. Chem. Phys. **126**, 074104 (2007).
[22] A. Jones, G.J. Martyna, J. Crain, M. Müser, and A. Thompson, Phys. Rev. B **79**, 144119 (2009).
[23] A.P. Jones, J. Crain, V.P. Sokhan, T.W. Whitfield, and G.J. Martyna, Phys. Rev. B **87**, 144103 (2013).
[24] P. Drude, *Lehrbuch der Optik* (S. Hirzelg, Leipzig, Germany, 1900).
[25] J.O. Hirschfelder, C.F. Curtiss, and R.B. Bird, *Molecular Theory of Gases and Liquids* (Wiley, New York, 1954).
[26] J. Morrone and R. Car, Phys. Rev. Lett. **101**, 017801 (2008).
[27] Y. Nagata, R.E. Pool, E.H.G. Backus, and M. Bonn, Phys. Rev. Lett. **109**, 226101 (2012).
[28] H. Goldstein, C. Poole, and J. Safko, *Classical Mechanics*, 3rd ed. (Addison-Wesley Boston, Boston, MA, 2001).
[29] A. Jones, F. Cipcigan, V.P. Sokhan, J. Crain, and G.J. Martyna, Phys. Rev. Lett. **110**, 227801 (2013).
[30] J. Jenson and M. Gordon, Mol. Phys. **89**, 1313 (1996).
[31] A.J. Stone, *The Theory of Intermolecular Forces* (Clarendon Press, Oxford, UK, 1996).
[32] C. Millot and A. Stone, Mol. Phys. **77**, 439 (1992).
[33] A. Warshel and M. Levitt, J. Mol. Biol. **103**, 227 (1976).
[34] J. Tersoff, Phys. Rev. B **37**, 6691 (1988).
[35] D.G. Pettifor and I.I. Oleinik, Phys. Rev. B **59**, 8487 (1999).
[36] M. Tuckerman, G. Martyna, M. Klein, and B. Berne, J. Chem. Phys. **99**, 2796 (1993).
[37] D. McQuarrie, *Statistical Mechanics* (Harper Collins, New York, 1976).
[38] R.P. Feynman, *Statistical Mechanics: A Set of Lectures* (Westview Press, Boulder, CO, 1998), p. 354.
[39] R.M. Wilcox, J. Math. Phys. **8**, 962 (1967).
[40] L.D. Fosdick and H.F. Jordan, Phys. Rev. **58**, 143 (1966).
[41] E.L. Pollock and D.M. Ceperley, Phys. Rev. B **2555**, 30 (1984).
[42] M. Parrinello and A. Rahman, J. Chem. Phys. **80**, 860 (1984).
[43] G.J. Martyna, M.L. Klein, and M. Tuckerman, J. Chem. Phys. **97**, 2635 (1992).
[44] A. Jones and B. Leimkuhler, J. Chem. Phys. **135**, 084125 (2011).
[45] E. Balog, A.L. Hughes, and G.J. Martyna, J. Chem. Phys. **112**, 870 (2000).

[46] G. Martyna, A. Hughes, and M. Tuckerman, J. Chem. Phys. **110**, 3275 (1999).
[47] U. Essmann, L. Perera, M.L. Berkowitz, T. Darden, H. Lee, and L.G. Pedersen, J. Chem. Phys. **103**(19), 8577 (1995).
[48] E. Pollock and J. Gloshi, Comp. Phys. Comm. **95**, 93 (1996).
[49] M. Herman, E. Bruskin, and B. Berne, J. Chem. Phys. **76**, 5150 (1982).
[50] W.L. Jorgensen, J. Chandrasekhar, J.D. Madura, R.W. Impey, and M.L. Klein, J. Chem. Phys. **79**, 926 (1983).
[51] S.W. deLeeuw, J.W. Perram, and E.R. Smith, Proc. R. Soc. London, Ser. **A 373**, 27 (1980).
[52] J. Hansen, *MD Dynamics Simulation of Coulomb Systems, in MD Simulation of Statistical Mechanical Systems* (North Holland, Amsterdam, 1986).
[53] M. Kalos and P. Whitlock, *Monte Carlo Methods* (Wiley-VCH, Berlin, 2008).
[54] S. Plimpton, J. Comp. Phys. **117**, 1 (1995).
[55] M. Tuckerman, G. Martyna, and B. Berne, J. Chem. Phys. **97**, 1990 (1992).
[56] G. Martyna, M. Tuckerman, D. Tobias, and M. Klein, Mol. Phys. **87**, 1117 (1996).
[57] D. Tobias, G. Martyna, and M. Klein, J. Chem. Phys. **101**, 4178 (1994).
[58] J.L.F. Abascal and C. Vega, Phys. Rev. Lett. **98**, 237801 (2007).
[59] B. Chen, J. Xing, and J.I. Siepmann, J. Phys. Chem. B **104**(10), 2391 (2000).
[60] I.F.W. Kuo, C.J. Mundy, B.L. Eggimann, M.J. McGrath, J.I. Siepmann, B. Chen, J. Vieceli, and D.J. Tobias, J. Phys. Chem. B **110**, 3738 (2006).
[61] T.D. Kühne, T.A. Pascal, E. Kaxiras, and Y. Jung, J. Phys. Chem. Lett. **2**, 105 (2011).
[62] K.R. Wilson, R.D. Schaller, D.T. Co, R.J. Saykally, B.S. Rude, T. Catalano, and J.D. Bozek, J. Chem. Phys. **117**, 7738 (2002).
[63] L.X. Dang and T.M. Chang, J. Chem. Phys. **106**(19), 8149 (1997).